International Journal of Chemistry; Vol. 9, No. 4; 2017
ISSN 1916-9698 E-ISSN 1916-9701
Published by Canadian Center of Science and Education

Creation of Hybrid Photoactive Inorganic/Organic Interface Assemblies of Cadmium Oxide mixtures (CdO_2/CdO)/Poly-2,2-Bithiophene; Optical and Photoelectrochemical Investigations

Kasem K. Kasem[1], Henry Worley[1], Ashley Lovins[1]

[1]School of Sciences, Indiana University Kokomo, USA

Correspondence: Kasem K. Kasem, School of Sciences, Indiana University Kokomo, USA.

Received: September 25, 2017 Accepted: October 15, 2017 Online Published: October 17, 2017

doi:10.5539/ijc.v9n4p71 URL: https://doi.org/10.5539/ijc.v9n4p71

Abstract

Nanoparticles of cadmium peroxide (CdO_2) were immobilized in poly 2,2 bithiophene (PBTh) to build photoactive inorganic/organic interfaces (I/O/I). Studies indicated that the CdO_2 initially immobilized in the organic polymer partially decomposed to a low band gap CdO. Therefore we refer to this mixture as CdO_2/CdO. The CdO_2/CdO/PBTh assemblies were subjected to optical and photoelectrochemical investigations in aqueous electrolytes containing acetate, nitrate, or phosphate. The equilibrium mixture of CdO_2/CdO influenced the optical conductivity and dielectric contents of the assemblies. Furthermore, O_2 played an important role in the charge separation and transfer processes. The effects of an applied magnetic field were investigated and reported. The results were explained on the basis of formation of hybrid sub-bands due to band alignments between the assembly components. The photo-induced charge generation of PBTh was improved by occlusion of CdO_2 in the polymer as was evident by the greater photocurrent generated by CdO_2/CdO/PBTh than that generated by PBTh.

Keyword: cadmium, photoelectrochemistry, bithiophene, interfaces, semiconductors, magnetism

1. Introduction

Transition metal peroxides can be used as a source of oxygen in organic synthesis. They can also be used in sensor building, and for catalysis (Zhou X.P. et al, 2003). Oxidation of aniline using cadmium oxide (CdO) has been reported (Karunakaran C. et al 2005). The high evaporation temperature of CdO, eliminates the toxicity risk of Cd-based oxides (Lu H.B. et al 2008). Polycrystalline thin films of cadmium oxide and cadmium titanate were prepared by the sol-gel method (ReYesa M.E. et al 2012), and further subjected to optical, structural, and crystalline property investigations. Several methods for preparation of CdO_2 were reported (Elmaghrabya E.K. et al 2014, Liu Y. et al 2009, Kavasoglu N. et al 2009, Xiaofei H. et al 2005, and Huffman C. W. W et al 1959).

Building hybrid interfaces such as at the hetero-junction of inorganic/organic (IOI) or organic/organic interfaces (OOI) is an effective method of surface modification. Controlled creation or elimination of surface defects can be achieved by building interfaces between photo-and catalytically-active materials. The charge production, separation, and transfer at these interfaces were the subject of several investigations (Akira T. et al 2011, Zing H.P. et al 2005, Braun X. S. et al 2007, Wan A. et al, 2005, Osikowiez W. et al 2007). The goal of this investigation was to decipher the alignment of energy bands at organic/organic or inorganic/organic interfaces.

Interfacing some transition metal oxides and chalcogenides with organic semiconductors was performed (Kasem K. et al, 2016 and 2017, Beck P et al 1992, Dela E.C. et al 2015). The moderate band gap of cadmium-based binary compounds is a promising property for the harvesting of solar radians in the visible range. Cadmium oxides have excellent optical and optoelectrical characteristics. They also have selective catalytic properties that make them suitable for use in industrial capacities such as the photodegradation of toxic organic compounds, dyes, pigments and other environmental pollutants (Karunakaran C. et al, 2009, Nezamzadeh-Ejhieh A. et al, 2011, and Saravanan R et al, 2011). The lack of photoelectrochemical studies on cadmium peroxide, CdO_2, drove our interest to explore the photoelectrochemical behavior of a photoactive cadmium oxides/poly-2,2-bithiophene or CdO_2/CdO/PBTh assembly.

In this work, the inorganic CdO_2/CdO nanoparticles were immobilized in a photoactive host organic polymer PBTh using the occlusion electrodeposition (OE) method. We investigated the extent to which the occlusion of CdO_2/CdO in PBTh influenced the photo-induced charge separation and further charge transfer process. Furthermore, we determined the optical parameters such as optical conductivity ($\sigma_{opt.}$), optical absorption coefficient (α), refractive index (n),

extinction coefficient (k), real dielectric constants (ε_r), and imaginary dielectric constants (ε_i). We explored the possible effects that can be caused by applying a magnetic field to the assembly.

2. Experimental

2.1 Reagents

All reagents were of analytical grade. All solutions were prepared using deionized (DI) water unless otherwise stated.

2.2 Preparations

2.2.1 CdO_2 Was Prepared According to Previously Published Procedure (Zhang Y. C et al 2008)

The I/O/I thin films were prepared as follows:

2.2.2 Preparation of CdO_2/CdO/PBTh Thin Films

The I/O/I thin films of CdO_2/CdO/PBTh were generated electrochemically using cyclic voltammetry (CV) by repetitive cycling of the FTO electrode potential between -0.5 and 1.7 V vs Ag/AgCl in an acetonitrile suspension of CdO_2/CdO, 1 mM of the BTh monomer and 0.5 M $LiClO_4$.

2.3 Instrumentation

All electrochemical experiments were carried out using a conventional three-electrode cell consisting of a Pt sheet as a counter electrode, Ag/AgCl as a reference electrode, and FTO as a working electrode with a 2 cm^2 surface area. Photoelectrochemical studies of the thin solid films were performed using experimental setup as illustrated in Figure 1. A BAS 100 W electrochemical analyzer (Bioanalytical Co.) was used to perform the electrochemical studies. Optical parameters were determined by the treatment of the steady state reflectance spectra generated by an Ez 2000 UV-VIS spectrophotometer. Irradiation was performed with a solar simulator 300-watt xenon lamp (Newport, NJ) with an IR filter. Magnetic measurements were performed using a Frederiksen digital Teslameter - 4060.50, with 0.01 - 2T, resolution 1mT.

2.4 Photolysis Cell

The electrolysis cell was a one-compartment Pyrex cell with a quartz window facing the irradiation source.

2.5 Measurement of Electron Life-Time (τ_n) at an Organic/Organic/Inorganic Interface

The following equation that relates $\boldsymbol{\tau_n}$ to the change in open circuit potential (V_{oc}) decay (Zaban A. et al 2003).

$$\tau_n = - (k_B T / e) * (dV_{oc} / dt)^{-1} \quad (1)$$

where k_B is the Boltzmann constant, e is the electron charge, T is the temperature in K, and $\mathbf{V}_{oc}$ is the open circuit potential, in Volt, was used

2.6 Magnetic Field Effects

Magnetic excitation was created by orienting the CdO_2/CdO/PBTh-coated FTO parallel to the magnetic field generated by two circular disk magnets with power of 0.200 T and facing the light source (Figure 1). The magnetic field was measured by placing the Tesla meter on the surface of the assembly before immersing it into the electrolyte. For comparison, the current and potential generated in the absence of the magnetic field were also measured.

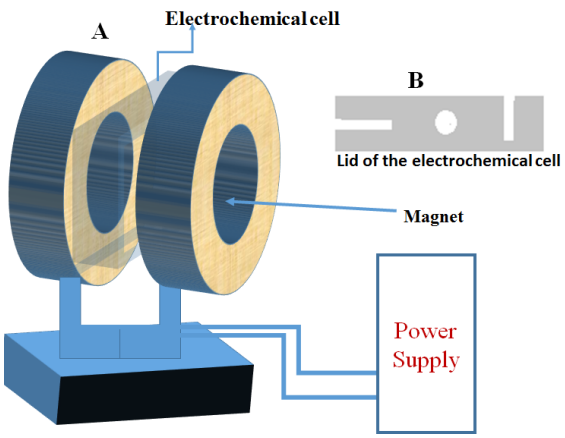

Figure 1. A) Magnetic field source applied on the electrochemical cell. B) The lid for the electrochemical cell provided the option of making the magnetic field parallel or perpendicular to the electrode surface

3. Results and Discussion

3.1 Optical Studies

Optical parameters such as $\sigma_{opt.}$, α, n, k, ε_r and ε_i have been calculated and plotted as a function of the photon energy. The results are displayed in Figures 2, 3, 4, 5 and 6.

3.1.1 Optical Band Gap of the Studied Assembly

The absorption spectra of the CdO_2/CdO/PBTh assembly and of the host polymer PBTh were studied in a wavelength range of 320-800 nm. The results are displayed in Figure 2A, a plot of absorption vs photon energy of incident light. The maximum absorption for the assembly was ≈ 3.40 eV (Figure 2A-a), which is consistent with the value of 3.48 eV reported by previous a study (De Leon-Gutierrez L.R. et al 2006). The large increase in the absorption started at ≈ 2.4 eV and continued until it reached a broader peak at 3.4 eV. The absorption at photon energies lower than 3.4 eV is due to the existence of CdO. The maximum absorption of PBTh alone is ≈ 2.5 eV (Figure 2A-a). Figures 2B & C plots of $\alpha^{½}$ vs photon energy (hν) and $(\alpha*h\nu)^2$ vs. hν respectively were prepared after treatment of the absorption data as described in previous studies (Tauc J. 1968). Figure 2B shows that the indirect band gap in PBTh is smaller than that of the assembly. This can be caused by creation of hybrid sub-bands due to the occlusion of CdO_2/CdO. These sub-bands have larger band gaps between the highest occupied molecular orbitals (HOMO) and lowest unoccupied molecular orbitals (LUMO) of the host polymer.

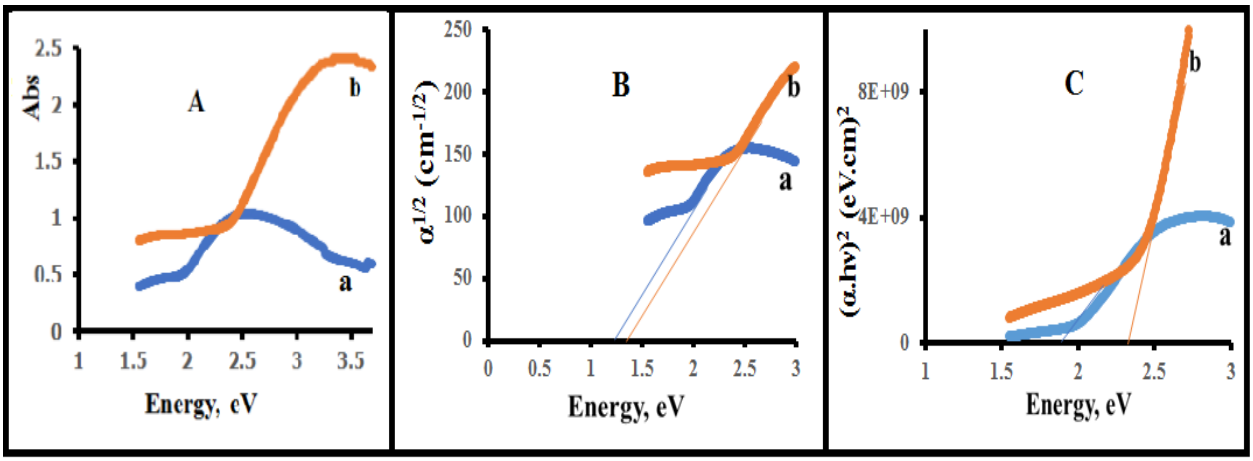

Figure 2. A) Absorption spectra; B) $\alpha^{½}$ ($cm^{-1/2}$) vs photon energy C) $(\alpha*h\nu)^2$, $(eV.cm)^2$ vs photon energy, a) PBTh and b) CdO_2/CdO/PBTh

Figure 2C indicates that the assembly shows an absorption band gap around 2.4 eV. This low band gap is closer to that reported for CdO. This indicates that the CdO_2 in the assembly underwent partial decomposition to produce CdO. The broad absorption peak in Figure 2Ab is caused the equilibrium mixture of CdO_2/CdO. The results also indicate that the absorbance range of the assembly is greater than that of the host polymer PBTh.

3.1.2 Optical Parameters

a) Refractive index, n, extinction coefficient, k

The relation of extinction coefficients k to photon energy are displayed in Figure 3A which clearly indicates that 1) the value of k for PBTh (trace a) is smaller than that of CdO_2/CdO/PBTh (trace b), 2) the value of k for PBTh increases with the increasing photon energy for PBTh up to ≈ 2.5 eV then decreases, and 3) the value of k for CdO_2/CdO/PBTh decreases up to ≈ 2.4 eV and then starts to increase. Figure 3B displays the relation of refractive index, n, to photon energy. PBTh shows a large increase in n between 2.0 and 2.4 eV, then remains unchanged at photon energies greater than 2.4 eV. On the other hand, the CdO_2/CdO/PBTh assembly shows a somewhat unchanged n within the 1.5 to 3.2 eV energy range. The assembly has a greater n value than the host polymer, PBTh, at photon energies lower than 2.0 eV and smaller n values than that of PBTh at photon energies greater than 2.0 eV.

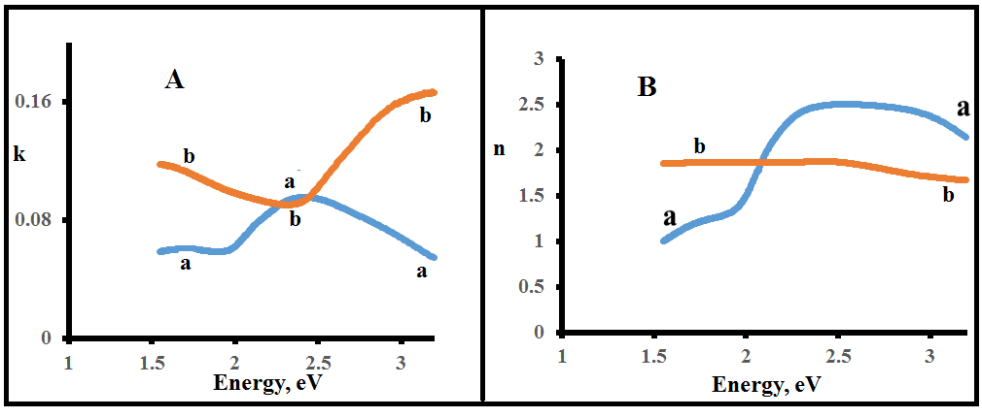

Figure 3. A) Extinction coefficient k, vs photon energy; B) Refractive index n vs photon energy a) PBTh and b) CdO_2/CdO/PBTh

b) Dielectric constants, real ε_r and imaginary ε_i:

Figure 4A displays the real component of the dielectric constant ε_r vs photon energy. This figure shows a pattern similar to that displayed in Figure 3B. This is because ε_r was calculated using the equation $\varepsilon_r = n^2-k^2$, where n >> k we can approximate the value of ε_r. Figure 3B displays the relation of ε_i to the photon energy. Figure 4A shows a resemblance to Figure 3A, due to the direct correlation of ε_i to the photon energy k ($\varepsilon_i = 2nk$).

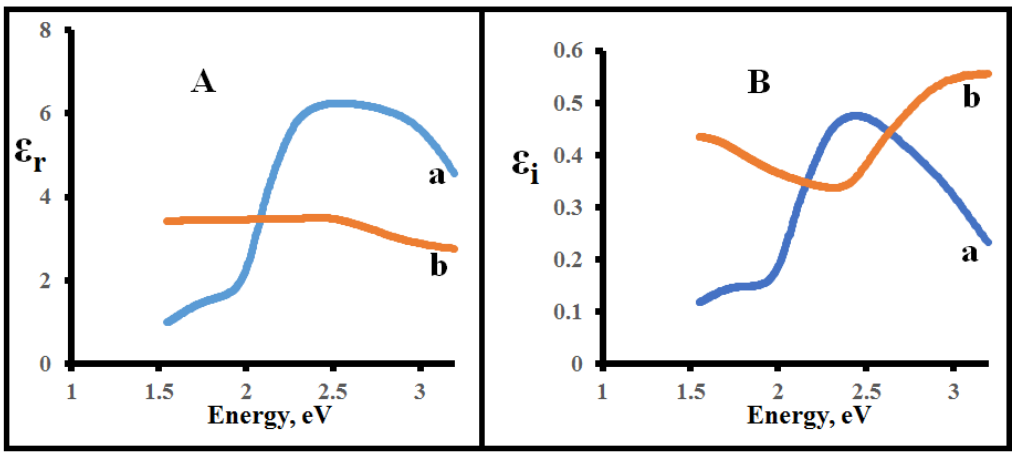

Figure 4. A) Real ε_r, and B) imaginary ϵ_i, components of dielectric constant. a) PBTh and b) CdO_2/CdO/PBTh

The results displayed in these figures show that: The ε_i of the CdO_2/CdO/PBTh assembly is greater than that calculated for PBTh (host polymer) except in the energy range between 2.2 and 2.7 eV where ε_i of the CdO_2/CdO/PBTh assembly is less than that of PBTh. Because ε_i is associated with dissipation of energy into the medium, it is possible that the occlusion of CdO_2/CdO nanoparticles into the network structure of PBTh enhanced the energy dissipation process (Dressel M. 2002) except in the range of photon energies that match the average band gap of the host polymer PBTh (2.2 -2.7 eV). The value of ε_i is an indication of the extent to which dielectric material absorbs energy from an electric field due to dipole motion. Furthermore, the results displayed in Figure 4A show that the real dielectric constant portion for CdO_2/CdO/PBTh is greater than that of PBTh up to 2.0 eV. Because the real portion of the dielectric constant is related to polarization and anomalous dispersion, it reflects the effects of occlusion of CdO_2/CdO on the speed of light traveling within the material (Sharma P. et al 2007). At photon energies greater than 2.0 eV, an opposite behavior was observed which reflects that CdO_2/CdO did not alter the speed of light after 2.0 eV.

The loss factor is the ratio between the imaginary and real parts of the dielectric constants ratios ($\varepsilon_i / \varepsilon_r$) which was calculated for both the PBTh and CdO_2/CdO/PBTh assemblies. Figure 5 displays the loss factor vs photon energy. It is quite clear that occlusion of CdO_2/CdO in the matrix of PBTh contributes to the increase of ε_i, and to the decrease of ε_r.

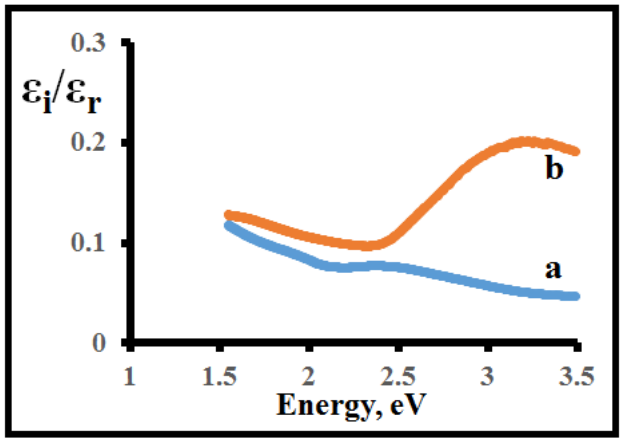

Figure 5. Loss factor (ε_i / ε_r) vs photon energy, a) PBTh and b) CdO_2/CdO/PBTh

c) The optical conductivity, σ_{opt}

The σ_{opt} values were calculated as described in previous work (Wu M.T. et al 1993). The results are displayed in Figure 6. The presence of CdO_2/CdO as a dopant in PBTh resulted in a decrease of optical conductivity (Figure 6b). This indicates that the dopant provides the host polymer with an additional charge transfer (Wu M.T. et al 1993) except in the 2.2-2.7 eV photon energy range that matches the PBTh band gap. The contribution of the dopant to the charge transfer process was explained on a basis that the reaction between incident light and charges of the material will take place as a result of absorption of photon energy by the assembly (Seraghni N. et al, 2012). The presence of CdO_2/CdO enhanced the process that leads to polarizing the charges of the material. This means that the CdO_2/CdO/PBTh positively affected the dissipation of energy into the host PBTh film. This is consistent with the results displayed for the imaginary-photon energy displayed in Figure 4B. Within the 2.2 -2.7 eV photon energy range the contribution of CdO_2/CdO to the polarization of charges in diffusive HOMO/LUMO of the host polymer did not take place.

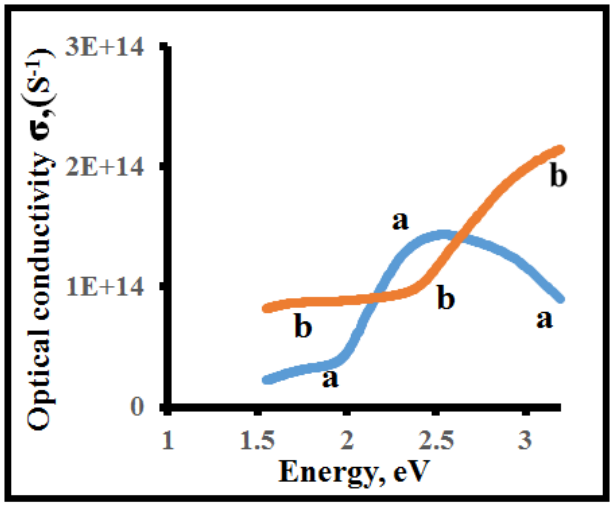

Figure 6. Optical conductivity vs photon energy a) PBTh, and b) CdO_2/CdO/PBTh

3.2 Photoelectrochemical Behavior

The optical and photoelectrochemical behaviors of the host polymer PBTh were discussed in previous work (Kasem K et al 2017). This information was used, for comparison to determine the contribution of the occluded CdO_2/CdO nanoparticles to the photo activity outcome of the entire assembly. Unless otherwise stated, the photoelectrochemical behavior was investigated by cycling the potential of FTO/ CdO_2/CdO/PBTh between -1.0 to 1.0 V vs. Ag/AgCl at a scan rate of 0.10 V/s in a given electrolyte both in the dark and under illumination.

3.2.1 Photoelectrochemical Behavior of the FTO/CdO_2/CdO/PBTh Assembly in Aqueous Acetate Electrolyte

The photoelectrochemical behavior of FTO/CdO_2/CdO/PBTh assemblies were investigated in an acetate electrolyte (pH = 8) in the dark and under illumination. Figure 7A, shows that in the cathodic scan at ≈0.40 vs Ag/AgCl. The recorded

photocurrent is greater than the current recorded in the dark. These results indicate that the approximate E_{fb} (flat band potential) of the assembly is at 0.40 V vs Ag/AgCl or 0.60 V vs SHE. (Table 1). However, in the anodic scan, the recorded photocurrent is smaller than that in cathodic scan and exceeds the current recorded in the dark at ≈ 0.10 vs Ag/AgCl. We assume that for acetate electrolyte, a 0.60 V vs SHE is the value of the hybrid sub-band created upon occlusion of CdO_2/CdO in PBTh thin film. Figure 7B shows the photocurrent vs time curve generated by subjecting the CdO_2/CdO/PBTh assembly to a constant potential (-0.8V vs Ag/AgCl) under illumination of long duration. Upon illumination of an oxygenated electrolyte, a sudden increase in the current (≈ 160 μA) occurred, followed by a large decrease in the photocurrent for 10 seconds after which the current increase again, reaching a steady state after 50 seconds of illumination (Figure 7B-a). The sharp current spear is an indication of fast charge recombination due to hole accumulations at the outermost layers of the assembly/electrolyte interface (Sookhakian M. et al 2014). When the electrolyte was subjected to a 0.2 T magnetic field in an oxygenated solution (Figure 7B-b) the background dark current was greater than that in the absence of a magnetic field (Figure 7Ba). However, upon illumination, the observed photocurrent was much lower than that in absence of a magnetic field. Figure 7C shows the photocurrent-time curve generated by subjecting the CdO_2/CdO/PBTh assembly to a constant potential (-0.8 V vs Ag/AgCl) under illumination of long duration in a deoxygenated electrolyte achieved by purging with N_2. Very little or negligible difference in the photocurrent was noted upon illumination of the assembly in the presence and absence of the magnetic field. However, the photocurrent generated by the assembly was much smaller than that recorded in presence of O_2. These observations, recorded in Figures 7 A, B and C, indicate that 1) the photocurrent curves generated in presence and in absence of O_2 indicate that O_2 plays an important role in enhancing charge separation during the illumination period (in absence of O_2 the photocurrent decreases) (Figure 7B and C), 2) the magnetic fields have tangible effects in presence of O_2 (Figure 7 B a,b), and 3) no magnetic field effects were found in absence of O_2 (Figure 7C). The paramagnetic nature of O_2 dissolved in the electrolyte and/or adsorbed on the surface of the electrode may have contributed to the observed outcome.

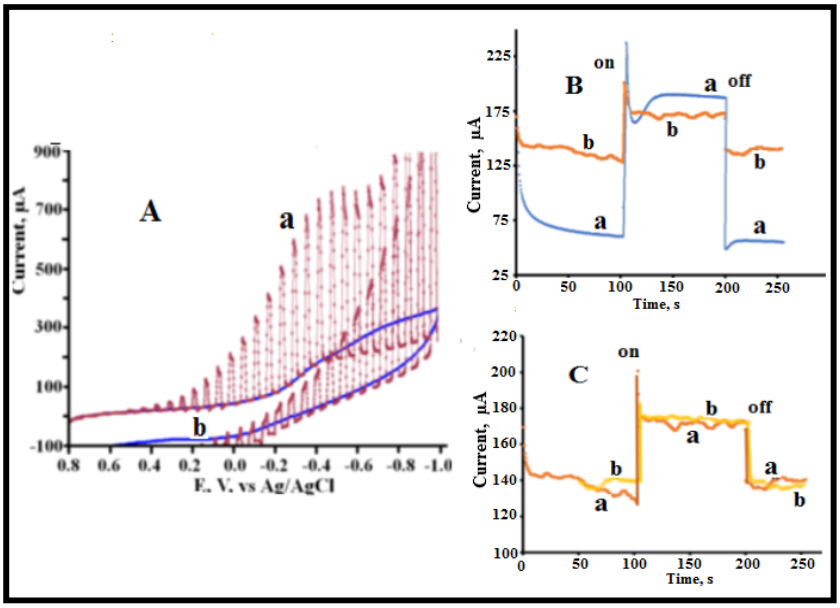

Figure 7. Photoelectrochemical behavior of FTO/CdO_2/CdO/PBTh in acetate electrolyte (pH = 8) a) illumination, b) dark; A) CV at 0.1 V/s; B) photocurrent -time curve at -0.5V vs Ag/AgCl, a) with O_2, b) with O_2 and magnet; C) photocurrent-time curve at -0.8 V vs Ag/AgCl, a) after purge with N_2, b) with N_2 and magnet

3.2.2 Electrochemical Behavior of the CdO_2/CdO/PBTh Assembly in Aqueous Nitrate Electrolytes (pH 7)

The photoelectrochemical behavior of FTO/CdO_2/CdO/PBTh assemblies were investigated in a nitrate electrolyte (pH 7) in the dark and under illumination. The results are displayed in Figures 8A and B. In the cathodic scan at ≈0.5V vs, Ag/AgCl the photocurrent is greater than the current recorded in the dark for a nitrate electrolyte (Figure 8A). We assume that 0.70 V vs SHE is the value of the hybrid sub-band created upon occlusion of CdO_2/CdO nanoparticles in PBTh in the nitrate electrolyte.

Figure 8B shows the linear sweep voltammetry (LSV) for CdO_2/CdO/PBTh in absence of and under the effect of a 0.2 T magnetic field. This figure illustrates that in the presence of the magnetic field (Figure 8B-b) not only was the photocurrent less than that in absence of magnetic field (Figure 8 B-a), but also that the dark-background current was greater than that in absence of magnetic field.

Figure 8C is a display of the photocurrent-time curve generated by subjecting the CdO_2/CdO/PBTh assembly to illumination under a constant potential (-0.620 V vs Ag/AgCl) in an oxygenated and deoxygenated electrolyte and in absence and presence of a 0.2 T magnetic field. Upon illumination of the oxygenated nitrate electrolyte (Figure 8C-a), a sudden increase in the current (300 µA) was followed by a large decrease in the photocurrent to about 120 µA trailed by steady small decrease to reach ≈ 100 µA. When the electrolyte was deoxygenated (Figure 8C-b), the illumination generated much less photocurrent (≈ 10 µA). This behavior was reproducible through multiple cycles of illumination and darkness. When a magnetic field was applied to the oxygenated electrolyte (Figure 8C-a') a sudden increase in photocurrent to about 140 µA followed by large decrease to about 70 µA in 20 s period occurred. Then the current reached a steady level of 50 µA. In the deoxygenated electrolyte (Figure 8C-b') no significant changes took place upon applying the magnetic field. Again the observed sharp current spear in Figure 8C is indication of fast charge recombination because of hole accumulations at the outermost layers of the assembly/electrolyte interface.

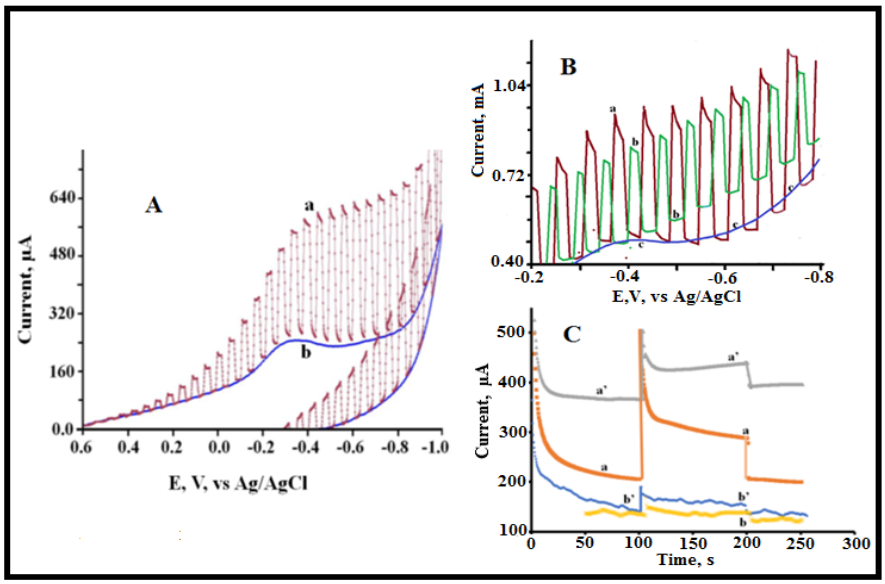

Figure 8. Photoelectrochemical behavior of CdO_2/CdO/PBTh in nitrate electrolyte A) CV at 0.1 V/s, a) illumination, b) dark; B) LSV at 0.1 V/s, a) no magnetic field, b) under 0.2 T magnetic field, c) dark (no magnetic field); C) photocurrent-time curve at -0.620 V vs Ag/AgCl, a) with O_2, a') with O_2 and magnetic field, b) after purge with N_2, and b') with N_2 and magnetic field

3.2.3 Electrochemical Behavior of the CdO_2/CdO/PBTh Assembly in Aqueous Phosphate Electrolyte

The photoelectrochemical behavior of CdO_2/CdO/PBTh in a phosphate electrolyte (pH 6) was investigated using procedure similar to that used for nitrate and acetate electrolytes. The results are displayed in Figures 9A and B. Figure 9A shows that at ≈ 0.4 V vs Ag/AgCl, the recorded photocurrent was greater than that recorded in the dark during the cathodic scan. The manual chopping of light indicates that the assembly is highly responsive to the illumination-dark cycles. The sudden decay of the photocurrent upon blocking the illumination every other second is an indication of a short life-time of the electron before its consumption into further elementary steps of photochemical reactions. Figure 9B shows the photocurrent-time curve which indicates the photo-activity at constant potential (-0.720 V vs Ag/AgCl) of this assembly under illumination for a longer period of time in absence (Figure 9B a, and b) and under the influence of a 0.2 T magnetic field (figure 9B a' and b'). Upon illumination of the oxygenated phosphate electrolyte, a sudden increase in the photocurrent (≈ 180 µA) was recorded (Figure 9B-a) followed by a steady decrease in photocurrent to about 70 µA. The initial decay reflects some e/h recombination. This behavior was reproducible through multiple cycles of illumination and darkness. In contrast, when the electrolyte was deoxygenated, less photocurrent was recorded (9B-b) with similar behavior to that observed in oxygenated solution. In presence of a magnetic field a small photocurrent was recorded (Figure 9B-a') followed by a decrease during a 30 s period after which the photocurrent started to increase to a constant value of ≈ 70 µA after a100 s illumination. The magnetic field in the absence of O_2 (Figure 9B, b') caused a very small increase in photocurrent upon illumination which maintained constant through the duration of 100 s illumination.

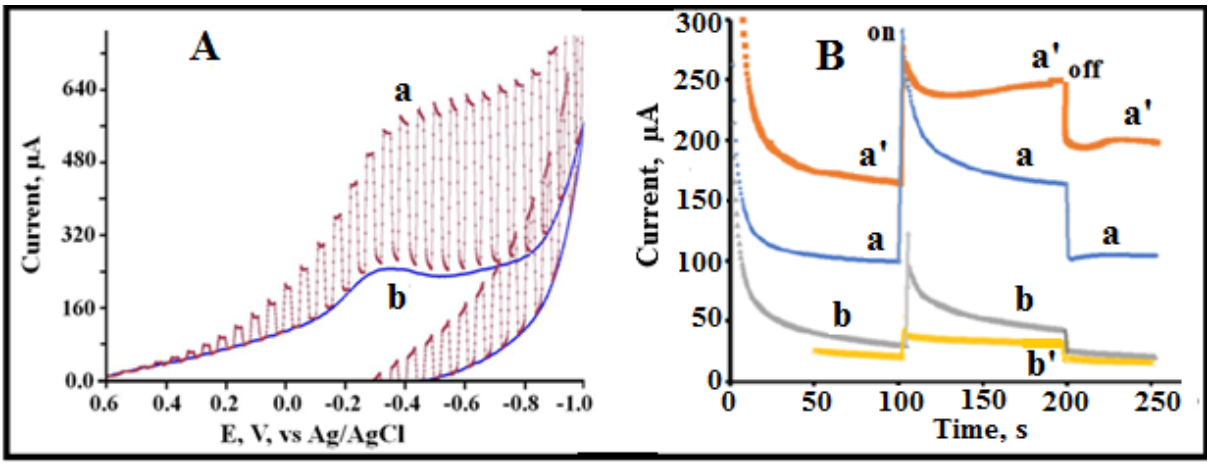

Figure 9. Photoelectrochemical behavior of CdO_2/CdO/PBTh in Phosphate electrolyte. A) CV at 0.1 V/s a) Illumination, b) dark; B) Photocurrent-Time curve at -0.72 V vs Ag/AgCl a) with O_2, and a') with O_2, and magnetic field, b) after purge with N_2 and b') N_2 and magnetic field

The electrochemical behavior of the host polymer PBTh in the 0.2 M phosphate electrolyte is recorded in Figure 10. Figure 10A clearly shows that PBTh generated much less photocurrent (maximum ≈ 290 µA) compared with that recorded (maximum ≈ 400 µA) for CdO_2/CdO/PBTh in phosphate (Figure 9 B). This indicates that occlusion of CdO_2/CdO enhanced the photo-induced charge separation as evident from the increase of the photocurrent in presence of CdO_2/CdO (Figures 9B, 10B).

In each electrolyte, no tangible change in the pH was observed even after 30 minutes of illumination. We further investigated the effect of changing the pH on the E_{fb} of this assembly. No changes in E_{fb} were observed within the pH 5-8 range.

The role of oxygen in the photochemical activities of the assembly in the studied electrolytes can be illustrated as follows:

$$O_2 + 2e + 2H^+ \rightarrow H_2O_2 \quad (2)$$

The hole consummation by the electrolyte's anions is an important step in the mechanism of charge separation.

In the presence of phosphate anion, formation of a phosphate radical anion is one way to prevent the e/h recombination process according to equation 3,

$$HPO_4^{-2}{}_{(aq)} + h \rightarrow HPO_4^{\cdot -}{}_{(aq)} \quad (3)$$

The formation of HPO_4^- has been reported (Mohammad A. et al 1990). Equations 2 and 3 explain how oxygen and phosphate participate in the charge separation process that lower the e/h recombination.

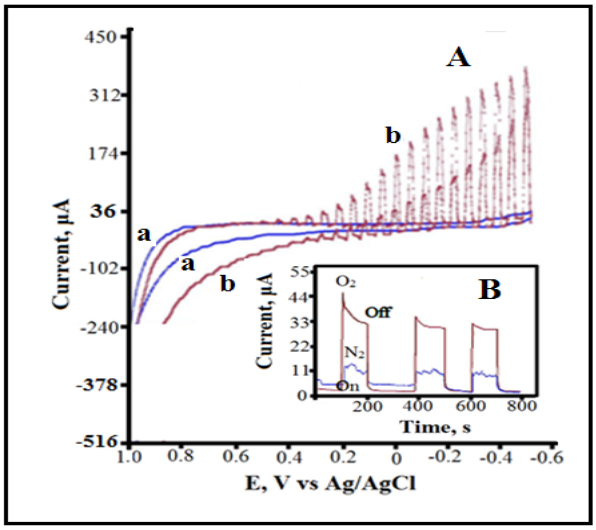

Figure 10. Photoelectrochemical behavior of PBTh in 0.2 M Phosphate electrolyte (pH 6). A) CV at 0.1 V/s, a) dark, b) Illumination; B) Photocurrent -Time curve at -0.6 V vs Ag/AgCl

In the presence of acetate electrolyte, the photooxidation of acetate results in a Kolb-type reaction. In the presence of $RCOO^-$ such as acetate, the following reaction takes place (Cervino R. M. et al 1984) as illustrated in equation 4.

$$R(COO^-)_{(aq)} + h \rightarrow R_{(aq)} + CO_{2\,(g)} \quad 4$$

Furthermore, in a nitrate electrolyte, oxidation of the nitrate anion to nitrate radical is possible and can be achieved by visible light energy (Hering T. et al 2015). This radical can be formed as shown in equation 5.

$$NO_3^-{}_{(aq)} + h \rightarrow NO_3^{\cdot} \quad 5$$

Reactions 3, 4, and 5 show how 0.2 M concentrations of these anions dominated the hole consumption and therefore increased the charge separation as indicated by the recorded large photocurrent in potentials more negative than 0.5 V vs Ag/AgCl.

3.2.4 Electron life-time (τ_n) at the Studied Assemblies

The changes in the open circuit potentials (dV_{opn}) of photoelectrochemical cells involved CdO_2/CdO/PBTh as a working electrode in acetates, nitrates, and phosphate electrolytes was applied to equation 1 from which an estimation of electron life-time at this interface in each electrolyte was made. The results are listed in Table 1. These data indicate that τ_n is shortest in acetate electrolyte and is longest in nitrate electrolyte. The longer electron life time (charge duration time) is related to the smaller change in the open circuit potential in the presence of the electrolyte. Reaction 2 took place during these electron-life times.

Table 1. Photoelectochemical data for the CdO_2/CdO/PBTh

Property	PBTh	CdO_2/CdO/PBTh	CdO_2/CdO
Ionization potential (IP), (EV)	5.65	5.65	6.31
Band gap, E_g, (eV)	2.55	2.50	3.48[a]
Electron Affinity (EA)	3.10	3.15	2.83
E_{fb},V vs SHE	0.50	≈0.6	Depends on doping
Electron-life time [a] (τ_n),s, in:			
1- Phosphate electrolyte		0.145	
2- Acetate electrolyte		0.087	
4- Nitrate Electrolyte		0.241	

[a] Calculated using equation 1.

3.2.5 Magnetic Field effect on the CdO_2/CdO/PBTh

The experimental set up for the magnetic study is displayed in Figure 1. The photocurrents of CdO_2/CdO/PBTh in the absence and in the presence of a magnetic field are displayed in Figures 7-9. These results suggest that oxygenated electrolytes are important factors in the response of the assembly to a magnetic field. Furthermore, the noticeable change in the CdO_2/CdO/PBTh photocurrent in the absence and presence of a magnetic field indicates that, upon illumination, unpaired electrons are generated. This creates organic paramagnetism with a random spin. The response of organic paramagnetism to the magnet depends on several factors such as the spin of electron/hole pairs, existence of singlet and triplet states, and interaction of donor anions (HPO_4^{2-}, NO_3^- and CH_3COO^-) with the excitons generated at this interface, and the intersystem crossing. The fact that a magnetic field has very little or no effect in absence of O_2 indicates that O_2 enhances the photocurrent in the absence of magnetic field, and interacts with an applied magnetic field in a way that generates less photocurrent. The presence of oxygen in the electrolytes contributed to a charge separation process by the formation of $O_2^{\bullet-}$. During its lifetime, this anion radical acted as a temporary molecular paramagnet (Seraghni N. et al 2012) that interfered with the applied a magnetic field and generated the recorded photocurrent outcome as shown in Figures 7-9.

3.3 Conclusion

The results obtained in this work indicate that occlusion of CdO_2 in PBTh improved the charge separation and consequently the generation of more photocurrent than was recorded for PBTh only. Nitrate electrolytes showed the longest electron-life time and consequently the longest electron diffusion length among the studied anions. Oxygenated electrolytes are important factors in the response of an assembly to a magnetic field. The optical properties of the assembly were changed dramatically in comparison to those of the host polymer PBTh. The data listed in Table 1, show that the assembly's energy band structure was manipulated by the host polymer structure.

Acknowledgment

The authors acknowledge financial support from Indiana University Kokomo.

References

Akira, T., Geng, Y. F., Wei, Q. S., Kazuhito, H., & Keisuke, T. (2011). Tailoring organic heterojunction interfaces in bilayer polymer photovoltaic devices. *Nature Materials, 10*, 450-455. https://doi.org/10.1038/nmat3026

Beck, P., Dahhaus, M., & Zahedi, N. (1992). Anodic codeposition of polypyrrole and dispersed TiO_2. *Electrochem. Acta, 37*, 1265. https://doi.org/10.1016/0013-4686(92)85066-T

Braun, X. S., Wojciech, O., Ying, W., & William, R. S. (2007). Energy level alignment regimes at hybrid organic–organic and inorganic–organic interfaces, *Organic Electronics, 8*(1), 14-20. https://doi.org/10.1016/j.orgel.2006.10.006

Cervino, R. M., Triaca, W. E., & Arvia, A. J. (1984). Phenomenology related to the kinetics of Kolbe electrosynthesis, *J. Electroanal. Chem., 172*, 255-264. https://doi.org/10.1016/0022-0728(84)80190-4

De La, C. T. E. C., Ambrosio, L. R. C., Mota, G. M. L., Luqueb, P. A., Castillo, S. J., & Carrillo-Castillo, A. (2015). A simple method for the synthesis of CdS nanoparticles using a Novel surfactant, *Chalcogenide Lett., 12*, 147-153.

De León-Gutiérrez, L. R., Cayente-Romero, J. J., Peza-Tapia, J. M., Barrera-Calva, E., Martínez-Flores J. C., & Ortega-López, M. (2006). Some physical properties of Sn-doped CdO thin films prepared by chemical bath deposition', *Materials Lett., 60*, 3866-3870. https://doi.org/10.1016/j.matlet.2006.03.131

Dressel, M. (2002). Electrodynamics of Solids Optical Properties of Electrons in Matter, George Grüner, Cambridge University press, Cambridge, UK. https://doi.org/10.1017/CBO9780511606168

Elmaghrabya, E. K., Kaidb, M. A., & Zakia, M. F. (2014). Optical Characterization of $(CdO)x(ZnO)_{1-x}$ Composite by Spray Pyrolysis Technique, *Acta Physica Polonica A, 125*, 82-86. https://doi.org/10.12693/APhysPolA.125.82

Hering, T., Slanina, T., Hancook, A., Wille, U., & Konig, B. (2015). Visible light photooxidation of Nitrate: the dawn of a nocturnal radical, *Chem. Comm., 51*, 6568-6571. https://doi.org/10.1039/C5CC01580D

Hoffman, C. W. W., Ropp, R. C., & Mooney, R. W. (1959). Preparation, properties, and structure of cadmium peroxide, *J. Am. Chem. Soc., 81*, 3830-3834. https://doi.org/10.1021/ja01524a008

Karunakaran, C., & Dhanalakshmi, R. (2009). Selectivity in photocatalysis by particulate semiconductors. *Cent. Eur. J. Chem. 7*, 134-137. https://doi.org/10.2478/s11532-008-0083-7

Karunakaran, C., & Senthilvelan, S. (2005). Semiconductor catalysis of solar photooxidation, *Curr. Sci., 88*, 962-967.

Kasem, K., Olsen, J. C., Baker, K, Santucci, C., Lalla, J., & Willman, A. N. (2016). Electrochemical studies on a photoactive. *Synthetic Metals, 217*, 61-67. https://doi.org/10.1016/j.synthmet.2016.03.013

Kasem, K., Elmasry, M., Baker, K., & Santucci, C. (2017). Photoelectrochemical and magnetic studies on photoactive interface thin film assemblies of poly bithiophene/poly 3-(2-thienyl) aniline/ferromagnetic Mg-doped Fe^2O^3 in aqueous electrolytes', *Thin Solid films, 634*, 56-65. https://doi.org/10.1016/j.tsf.2017.05.016

Kavasoglu, N., Kavasoglu, A. S., & Oktik, S. (2009). *J. Phys. Chem. Solids, 70*, 521. https://doi.org/10.1016/j.jpcs.2008.11.018

Liu, Y., Zhan, Y. C., & Xu, X. F. (2009). Hydrothermal synthesis and photocatalytic activity of CdO_2/CdO nanocrystals. *J. Hazardous Mater. 163*, 1310. https://doi.org/10.1016/j.jhazmat.2008.07.101

Lu, H. B., Liao, L., Li, H., Tian, Y., Wang, D. F., Li, J. C., … Wu, Y. (2008). Fabrication of CdO nanotubes via simple thermal evaporation, *Mater. Lett., 62*, 3928-3930. https://doi.org/10.1016/j.matlet.2008.05.010

Mohammad, A., Gary, K., Low, C., & Matthews, R. W. (1990). Effects of common inorganic anions on rates of photocatalytic oxidation of organic carbon over illuminated titanium dioxide, *J. Phys. Chem., 94*, 6820-6825. https://doi.org/10.1021/j100380a051

Nezamzadeh-Ejhieh, A., & Banan, Z. (2011). A comparison between the efficiency of CdS Nanoparticles/zeolite A and CdO/zeolite A as catalysts in photodecolorization of Crystal Violet. *Desalination, 279*, 146-151. https://doi.org/10.1016/j.desal.2011.06.006

Osikowicz, W., Salaneck, W. R., & de Jong, M. P. (2007). Formation of the Interfacial Dipole at Organic-Organic Interfaces: C_{60}/Polymer Interfaces"*Advanced Materials, 19*, 4213-4217. https://doi.org/10.1002/adma.200700622

Reyesa de Anda, M. E., Torres, D. G., Castanedo, P. R., Marquez, M. J., & Zelaya, A. O. (2012). J. Photochem. Photobiol. A: Chem., *228*, 22-27. https://doi.org/10.1016/j.jphotochem.2011.11.007

Saravanan, R., Shankar, H., Prakash, T., Narayanan, V., & Stephen, A. (2011). ZnO/CdO composite nanorods for photocatalytic degradation of methylene blue under visible light. Mater. *Chem. Phys. 125*, 277-280. https://doi.org/10.1016/j.matchemphys.2010.09.030

Seraghni, N., Belattar, S., Mameri, Y., Debbache, N., & Sehili, T. (2012). Fe(III)-Nitrate-Complex-Induced Photooxidation of 3-Methylphenol in Aqueous Solution. *Int. J. Photoenergy*. https://doi.org/10.1155/2012/630425

Sharma, P., & Katyal, S. C. (2007). J. Phys. D, Determination of optical parameters of alfa $(As_2Se)_{90}$ Ge_{10} thin film. *Applied physics, 40*, 2115-2120.

Sookhakian, M., Amin, Y. M., Baradaran, S., Tajabadi, M. T. A., Moradi, A., Golsheikh, A., & Basirun, W. J. (2014). A layer-by-layer assembled graphene/zinc sulfide/polypyrrole thin-film electrode via electrophoretic deposition for solar cells' *Thin Solid Films*, 204-211. https://doi.org/10.1016/j.tsf.2013.12.019

Tauc, J. (1968). Optical properties and electronic structure of amorphous Ge and Si. *Materials Research Bulletin. 3,* 37-46. https://doi.org/10.1016/0025-5408(68)90023-8

Wan, A., Hwang, J., Amy, F., & Kahn, A. (2005). Impact of electrode contamination on the α NPD/Au hole injection barrier. *Org. Electron., 6*, 47. https://doi.org/10.1016/j.orgel.2005.02.003

Wu, M. T., Yao, X., Yuan, Z. H., Sun, H. T., Wu, W. C., Chen, O. H., & Xu, G. Y. (1993). Effect of noble metal catalyst on titania exhaust gas oxygen sensor. *Sensors and Actuators B, 14*, 491. https://doi.org/10.1016/0925-4005(93)85060-N

Han, X. F., Liu, R., Xu, Z. D., Chen, W. X., & Zheng, Y. F. (2005). Room temperature deposition of nanocrystalline cadmium peroxide thin film by electrochemical route Electrochem. *Commun. 7*, 1195-1198. https://doi.org/10.1016/j.elecom.2005.08.023

Zaban, A., Miri, G., & Juan, B. (2003). Determination of the electron life time in monocrystalline dye solar cells by open –circuit voltage decay measurements. *Chem. Physics. Chem, 4,* 859. https://doi.org/10.1002/cphc.200200615

Zeng, H. P., Wang, T. T., Sandanayaka, S. D., Araki, Y., & Ito, O. (2005). Photoinduced Charge Separation and Charge Recombination in [60]Fullerene-Ethylcarbazole and C6 Fullerene-Triphenylamines in Polar Solvents. *J. Phys. Chem. A, 109*, 4713-4720. https://doi.org/10.1021/jp050914d

Zhou, X. P., Yilmaz, A., Yilmaz, G. A., Lorkovic, I. M., Laverman, L. E., Weiss, M., … Ford, P. C. (2003). *Chem. Commun., 1*, 2294. https://doi.org/10.1039/b307235e

Zhang, Y. C., Wang, G. L., Hu, X. Y., & Zhou, W. D. (2008). Temperature solid-phase synthesis of pure $CdTiO_3$ submicrocrystals using CdO_2/CdO nanoparticles as a precursor. *J. Cryst. Growth, 310*, 724. https://doi.org/10.1016/j.jcrysgro.2007.11.085